

# Spectral properties and phase diagram of correlated lattice bosons in an optical cavity within the B-DMFT

Jaromír Panas,<sup>1</sup> Anna Kauch,<sup>2</sup> and Krzysztof Byczuk<sup>1</sup>

<sup>1</sup>*Institute of Theoretical Physics, Faculty of Physics,*

*University of Warsaw, Pasteura 5, 02-093 Warszawa, Poland*

<sup>2</sup>*Institute of Physics, Academy of Sciences of the Czech Republic, Na Slovance 2, 18221 Praha, Czech Republic*

(Dated: December 9, 2024)

We use the Bose-Hubbard model with an effective infinite-range interaction to describe the correlated lattice bosons in an optical cavity. We study both static and spectral properties of such system within the bosonic dynamical mean-field theory (B-DMFT), which is the state of the art method for strongly correlated bosonic systems. Both similarities and differences are found and discussed between our results and those obtained within different theoretical methods and experiment.

## I. INTRODUCTION

The development of experiments with cold quantum gases in optical lattices<sup>1,2</sup> led to a breakthrough in the studies of strongly correlated systems. Its close correspondence with the Bose-Hubbard model, together with the possibility of fine-tuning of the parameters of the system gives a remarkably powerful tool for investigating quantum phenomena in this model.<sup>3</sup> On the other hand, the fast growing field of research on cold atoms in cavity-generated optical potential gives us a good understanding of processes in which atoms interact with radiation field.<sup>4</sup> Combining these two fields of research together opens up a possibility of a new fascinating study. Putting an optical lattice inside an optical cavity results in an effective infinite-range interaction between particles in the system.<sup>5</sup> This long-range interaction, mediated by the cavity mode of the light, competes with the inherent short range interaction of the Bose-Hubbard model. As a result of this competition between correlations on different length scales, new states of matter emerge. On top of the phases of the Mott insulator (MI) and superfluid (SF), known from theoretical predictions<sup>6</sup> and confirmed in experiment<sup>1</sup>, we expect new phases of density wave (DW) and supersolid (SS).<sup>7</sup>

Recent experiment with lattice bosons in an optical cavity<sup>5</sup> has stimulated a lot of theoretical research on this subject. In several published papers, the Bose-Hubbard model with infinite-range interaction has been studied within the static mean-field theory.<sup>8,9</sup> These studies include results for the phase diagram of such a system and some initial results for low energy spectra. However, these mean-field type approaches treat the kinetic term of the Hamiltonian as a small perturbation. A more advanced way, to study the Bose-Hubbard model with infinite-range interaction would be to use the bosonic dynamical mean-field theory (B-DMFT).<sup>10</sup> Such an approach allows us to obtain reliable results for any ratio of kinetic and potential energies. First application of the B-DMFT to a system with the optical lattice inside an optical cavity was presented in Ref. 7, in which DW and SS phases were obtained.

In this paper we aim to expand on the previous B-

DMFT study. We obtain the phase diagram and discuss the spectral properties of the Bose-Hubbard model with infinite-range interaction. Instead of performing calculations in real-space we consider an infinite system and derive an appropriate self-consistency condition for a bipartite lattice in two dimensions. Using the B-DMFT instead of the static mean-field approach gives us access to dynamical properties and a better approximation for small values of the local interaction. We observe similarities between these methods but also significant discrepancies, revealed in the behavior of the system close to the phase transition between the SS and DW phases and in the properties of the SS phase.

This paper is organized as follows. In Sec. II we introduce the Bose-Hubbard model with infinite range interaction and present the B-DMFT method together with its new self-consistency relations, appropriate for a bipartite lattice (full equations are included in App. A). We discuss some issues related to using a self-consistent approach in the studied problem in Sec. II C. In Sec. III A we present the phase diagram of the system, compare it to the one obtained within the static mean-field approach and discuss differences between the results of the two approaches. In Sec. III B we present the local densities of states and momentum resolved spectral functions and discuss their features. In Sec. IV we provide the summary of our results.

## II. MODEL AND INVESTIGATION METHOD

### A. The Bose-Hubbard model with cavity mediated infinite-range interaction

We consider a system with cold-atom quantum gas trapped in an optical lattice which is additionally placed inside an optical cavity. Such a setup was recently realized in experiment.<sup>5</sup> The counter-propagating laser beams of wavelength  $\lambda$  create a standing wave. This results in an effective periodic potential, which has the periodicity equal to half of the wavelength of the light beam,  $\lambda/2$ . We consider a two dimensional (2D) realization of such a system in the  $xz$  plane. The laser beam in the  $z$

direction plays a second role as it drives a cavity mode in the  $x$  direction through scattering of light on atoms in the system. The scattering processes between atoms and the cavity light creates a  $\lambda$ -periodic modulation of the optical-lattice potential. Theoretical treatment of such experiments requires a complex analysis of a system with many degrees of freedom: (i) *internal atomic degrees of freedom* - processes of exciting an electron in an atom (it is justified to treat an atom as a two state system<sup>4</sup>), (ii) *a light mode in the cavity degrees of freedom* - processes of creating and annihilating photons in the cavity due to the scattering of photons on atoms, (iii) *motional degrees of freedom* - an atom moving through the system, hopping from one potential well to a neighboring one.<sup>4</sup> Within dispersive limit, when atomic saturation effects are negligible and atoms are considered as linearly polarizable particles, one can get rid of atomic internal degrees of freedom.<sup>4</sup> If the decay rate of photons from the cavity is large we can adiabatically eliminate the cavity field. Then we obtain an effective Hamiltonian with an infinite-range interaction mediated by the cavity mode in the following form<sup>5</sup>

$$\hat{H} = - \sum_{i,j} t_{ij} \hat{b}_i^\dagger \hat{b}_j - \mu \sum_i \hat{b}_i^\dagger \hat{b}_i + \frac{U}{2} \sum_i \hat{b}_i^\dagger \hat{b}_i^\dagger \hat{b}_i \hat{b}_i - \frac{V}{N} \left( \sum_{i \in S_A} \hat{b}_i^\dagger \hat{b}_i - \sum_{i \in S_B} \hat{b}_i^\dagger \hat{b}_i \right)^2, \quad (1)$$

where  $\hat{b}_i^\dagger$  ( $\hat{b}_i$ ) is a bosonic creation (annihilation) operator on a lattice site  $i$ ,  $\mu$  is the chemical potential,  $U$  is the local interaction strength, and  $t_{ij}$  is the hopping amplitude. The first three terms represent the Bose-Hubbard Hamiltonian for which we assume nearest neighbor (NN) hopping, i.e.,  $t_{ij} = t > 0$  if sites  $i$  and  $j$  are NN and  $t_{ij} = 0$  otherwise. These terms alone describe a homogeneous isotropic square lattice and would correspond to a system without the cavity field. The last term in the Hamiltonian represents an effective infinite-range interaction, mediated by the cavity field. Such an interaction splits the square lattice into two sublattices  $A$  and  $B$ . The parameter  $V$  controls the strength of this interaction.  $S_A$  and  $S_B$  denote sets of site indices corresponding to the sublattices  $A$  and  $B$ , respectively. Because of the  $N^{-1}$  term in the last part of the Hamiltonian (1) the fluctuations are negligible for this type of interaction in the thermodynamic limit. Therefore it is sufficient to treat the last term of (1) within a mean-field approach, which leads to the following Hamiltonian

$$\hat{H} = - \sum_{i,j} t_{ij} \hat{b}_i^\dagger \hat{b}_j - \mu \sum_i \hat{b}_i^\dagger \hat{b}_i + \frac{U}{2} \sum_i \hat{b}_i^\dagger \hat{b}_i^\dagger \hat{b}_i \hat{b}_i - V \left( \sum_{i \in S_A} \hat{b}_i^\dagger \hat{b}_i - \sum_{i \in S_B} \hat{b}_i^\dagger \hat{b}_i \right) (n_A - n_B) + NV \frac{(n_A - n_B)^2}{4}, \quad (2)$$

where  $n_A$  ( $n_B$ ) is the average occupation of a site on the sublattice  $A$  ( $B$ ). The last term is important for the correct determination of the phase transition lines.

The Hamiltonian (2), is of the form of the Bose-Hubbard model with the addition of an effective staggered mean-field, resulting in a bipartite lattice. The values of  $n_A$  and  $n_B$  are determined self-consistently. Although the problem has been simplified, it still poses a considerable challenge to solve. Selected results, which are obtained within the static mean-field approximation, have been recently presented by Y. Chen *et al.* in Ref. 8 and by N. Dogra *et al.* in Ref. 9. In our paper we use the B-DMFT<sup>10</sup> approximation to solve this problem. The previous studies showed that this method is well suited for studying the Bose-Hubbard type models.<sup>11-14</sup> It has also been applied to a model of a finite system inside the optical cavity.<sup>7</sup> We expand this research to infinite homogeneous system and present a more detailed study.

## B. B-DMFT for a bipartite lattice

In the DMFT the self-energy is approximated to be momentum independent.<sup>15</sup> This allows to map a lattice problem onto an effective local (“impurity”) problem with additional self-consistency conditions. A detailed derivation for the case of bosons can be found in Ref. 10. However, for a bipartite lattice we have two distinct types of sites and, therefore, we need to solve two impurity problems and modify the self-consistency conditions appropriately. The impurity action for the sublattices  $A$  and  $B$  reads

$$S_{A/B}^{loc} = \int_0^\beta d\tau b^*(\tau) [\partial_\tau - \mu \mp V(n_A - n_B)] b(\tau) + \frac{U}{2} \int_0^\beta d\tau b^*(\tau) b^*(\tau) b(\tau) b(\tau) - \kappa \int_0^\beta d\tau \Psi_{(A/B)}^*(\tau) \mathbf{b}(\tau) + \frac{1}{2} \int_0^\beta d\tau \int_0^\beta d\tau' \mathbf{b}^*(\tau) \Delta_{(A/B)}(\tau - \tau') \mathbf{b}(\tau'), \quad (3)$$

where  $(-)$  sign is for the sublattice  $A$  and  $(+)$  sign for the sublattice  $B$ . Notation for other parameters is the same as in Ref. [16]:  $\beta = 1/T$  is inverse of temperature,  $\kappa = zt$ ,  $z = 4$  is the number of nearest neighbors on the square lattice,  $\tau$  is the imaginary time and

$$\mathbf{b} = \begin{pmatrix} b \\ b^* \end{pmatrix} \quad (4)$$

are the complex variables in the Nambu notation.<sup>17</sup> The action (3) resembles the action in a homogeneous problem,<sup>16</sup> however, the vector  $\Psi$  and the matrix  $\Delta$  vary between the sublattices. These external fields are: (i) the Bose-Einstein condensate (BEC) on a lattice with a cavity (a site removed), represented by a  $\tau$ -independent

mean field  $\Psi$ , and (ii) the dynamical mean field of non-condensed bosons, represented by a matrix of hybridization functions  $\Delta$ . The values of the latter are given by

$$\Delta_{(A/B)}(\tau - \tau') = - \sum_{i,j \neq 0} t_{i0} t_{j0} \langle T_\tau \hat{\mathbf{b}}_i(\tau) \hat{\mathbf{b}}_j^\dagger(0) \rangle_{(A/B)}^{(0)}, \quad (5)$$

where  $\langle \dots \rangle_{(A/B)}^{(0)}$  stands for the *connected* part of the equilibrium average in the grand canonical ensemble, and where site 0 is removed, creating an impurity which resides on the sublattice  $A$  or  $B$ , respectively.  $\hat{\mathbf{b}}^\dagger = (\hat{b}^\dagger, \hat{b})$  is the Nambu vector notation for the creation and annihilation operators.  $T_\tau$  represents the time ordering of operators. Similarly the condensate fields are

$$\Psi_{(A/B)} = \langle \hat{\mathbf{b}} \rangle_{(A/B)}^{(0)}. \quad (6)$$

We see that the local action (3) contains three quantities that depend on the properties of the lattice sites surrounding the impurity, i.e.,  $\Delta_{A/B}$ ,  $\Psi_{A/B}$  and  $n_{A/B}$ . Their values are obtained from the local quantities in a self-consistent way. It is done by using the Dyson equation within the B-DMFT approximation for the self-energy. In Appendix A we show how to calculate the Green function for a full lattice if the self-energy is momentum independent within each of the sublattices but varies between them.

The solution of the impurity problem (3) is the most demanding step in the B-DMFT self-consistency loop. In this paper we use the continuous-time quantum Monte Carlo (CT-QMC)<sup>18,19</sup> method as a single impurity solver.<sup>13,14</sup> It is a stochastic method, which does not impose any extra approximations. Within this approach one can, in principle, obtain arbitrary accuracy of the results with the main limitation coming from computation time.

### C. Metastability and phase transition line

A characteristic feature of a self-consistent iterative method is that the converged solution might depend on the initial condition, from which the iteration starts. In particular, depending on how one performs calculations the phase space parameters at which a phase transition occurs might be different. This is not the case for the phase transition between MI and SF phases for the model (1). However, this issue does influence other phase transitions which we study in this paper. This might be easily understood in the atomic limit (hopping amplitude  $t$  is set to zero) for zero temperature and for  $\mu = 0.4U$ , as an example. In such case it is possible to solve the original lattice problem (1). There are two states that are candidates for the ground state. The average value of the Hamiltonian has local minimum with respect to small variations from these two states. One state corresponds to the MI with average occupation  $n_A = n_B = 1$  and one

corresponds to the DW with  $n_A = 2$  and  $n_B = 0$ . The physical solution is the one with lower value of the grand potential, which in the zero temperature is  $\langle \hat{H} \rangle$  (notice, that the chemical potential  $\mu$  has been included in the Hamiltonian (1)). Thus we obtain a phase transition between MI and DW at  $V = 0.5U$ . However, if we consider a problem mapped onto a single impurity and treat it in a self-consistent manner<sup>20</sup> we get a DW phase stable down to  $V = 0.3U$ . This is because for  $0.5U > V > 0.3U$  the DW is a metastable solution. Similarly, for  $V > 0.5$  it is possible for self-consistent steps to converge to a MI solution, even though it has a higher value of the grand potential than the DW solution.

Therefore, solving the B-DMFT equations self-consistently is not enough to determine the phase diagram. In order to determine the physically true phase for a given set of parameters one needs to compare values of the grand potential for all of the metastable solutions. Here we revert to an approximate scheme of calculating the grand potential  $\Omega$  by assuming that  $\Omega \approx \langle \hat{H} \rangle$ . This approximation is equivalent to neglecting the entropic contribution  $-TS$ , which becomes formally rigorous only in the zero temperature limit. We checked within the static mean-field approximation<sup>6</sup> that the neglected term is small compared to the internal energy, owing to the low temperatures in which we performed calculations ( $TS \sim 10^{-3} \langle \hat{H} \rangle$ ), hence the approximation, in which the  $-TS$  term is neglected, is justified.

## III. RESULTS

### A. Phase diagram and static properties

Our main goal is to expand the previous B-DMFT study of a two-dimensional system in an optical cavity.<sup>7</sup> This is achieved by determining a phase diagram in the  $(t, V)$  space and comparison with the results of the static mean-field study.<sup>8</sup> These diagrams are presented in Fig. 1: the B-DMFT results – top panel, and the static mean-field results – bottom panel. The parameters for which we performed calculations are  $U = 10$ ,  $\mu = 4$ ,  $\beta = 2$ . In order to make a distinction between different phases we define two order parameters: any of the  $\phi_{(A/B)} = \langle \hat{b}_{(A/B)} \rangle$  fields (a situation, in which only one of them is (non-)zero is impossible), and  $\Delta n = n_A - n_B$ . These two order parameters allow us to define four phases: Mott insulating (MI), superfluid (SF), density wave (DW) and supersolid (SS) phases, as follows

- the Mott insulating phase is characterized by vanishing of both order parameters, i.e.,  $\phi_A = \phi_B = 0$  and  $\Delta n = 0$ . In this phase particles are immobile at  $t = 0$ , localized on lattice sites and distributed uniformly in the system.
- the superfluid phase is characterized by the presence of the condensed bosons in the system, where

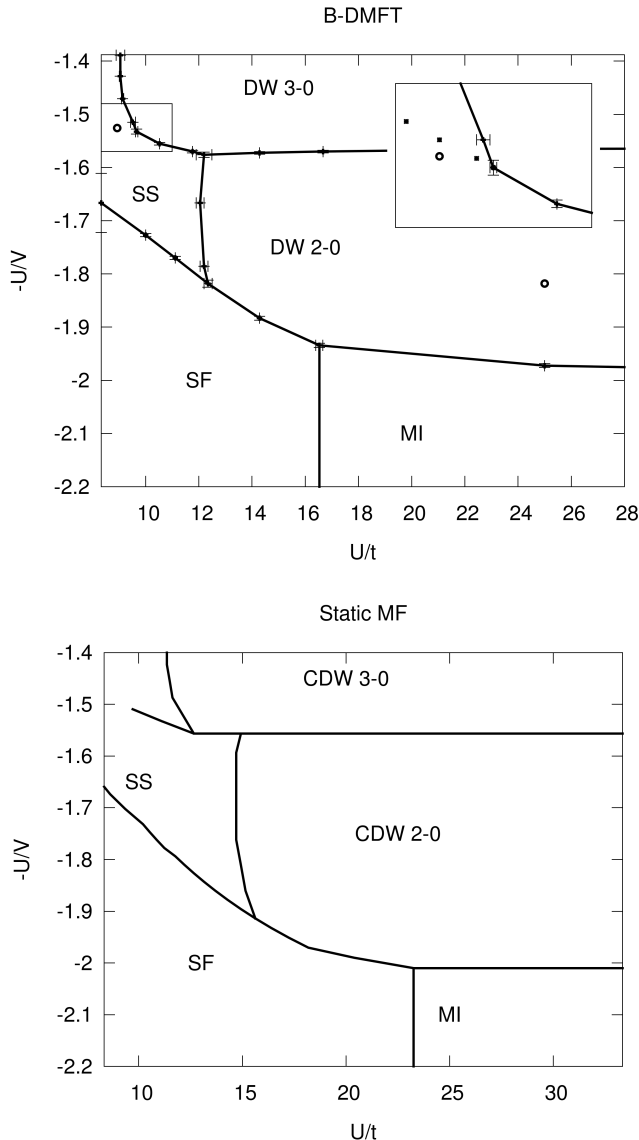


FIG. 1. Phase diagram of the two-dimensional system described by Hamiltonian (1). Parameters are set to  $U = 10$ ,  $\mu = 0.4U$  and  $\beta = 2$ . Distinct phases are denoted: MI—Mott insulator; SF—superfluid; DW 2-0—density wave with  $n_A \approx 2$  and  $n_B \approx 0$ ; DW 3-0—density wave with  $n_A \approx 3$  and  $n_B \approx 0$ ; SS—supersolid. Top panel: results obtained within the B-DMFT method. The inset shows a close up of the area marked with rectangle. Empty circles denote parameters, for which the spectral functions are determined. Small dots in the inset denote kinks in the dependence of  $\phi_A - \phi_B$  on  $V$ . Bottom panel: results obtained within the static mean-field method.

$\phi_{(A/B)} \neq 0$ , and the uniform distribution of particles in it, i.e.,  $\Delta n = 0$ .

- the density wave is defined by  $\Delta n \neq 0$  and  $\phi_A = \phi_B = 0$ . There are no condensed bosons in the system, however, the symmetry between sublattices is spontaneously broken.

- the supersolid phase is obtained when both order parameters are non-zero. There are two simultaneously broken symmetries,  $\mathbb{Z}_2$  between the sublattices and  $U(1)$  for the phase of the macroscopic wave function of the condensate.

Within the DW phase we find yet another two phases differing in the approximate value of  $\Delta n$ : DW 2-0 with  $\Delta n \approx 2$  in which sublattice  $A$  is on average occupied by approximately 2 particles per site, and DW 3-0 for which  $\Delta n \approx 3$  and sublattice  $A$  is on average occupied by approximately 3 particles per site. Sublattice  $B$  is almost empty in both cases. In general we expect more DW type phases for different parameters of the system,  $V$ ,  $\mu$ , etc. The phase transition between such phases is signaled by a discontinuity of  $\Delta n$ , here as a function of infinite-range interaction strength  $V$ . Apart from the difference in  $\Delta n$  the two phases appearing in the diagram in Fig. 1 are similar in their properties and symmetry.

A comparison between the results of the experiment<sup>5</sup> and the different theoretical approaches<sup>8,9</sup> shows certain similarities. We find the same type of phases in both approaches. The shapes of the diagrams are also similar. E.g., consider the phase transition line which separates MI from DW for small hopping amplitude and SF from SS for large. As we go along this line from large to small values of  $t$  it descends and then flattens out. The SF extends to higher values of  $V$  than the MI. This is a common feature of both experimental and theoretical results. However, there is also an important disagreement between the theories and the experiment. The interpretation of experimental results suggests that there exists a point in the phase-space in which all four phases meet, c.f., Fig. 3 of Ref. 5. In our phase diagram, and similarly in the phase diagrams obtained within the static mean-field approximation,<sup>8,9</sup> such a point does not exist. The Mott insulating and supersolid phases are always separated by the density wave and superfluid phases.

We also find discrepancies between the B-DMFT and the static mean-field results. Firstly, there is a difference in the shape of the phase transition line between the DW and MI phases. In the bottom panel of Fig. 1 we see, that this transition appears for a constant value of  $-U/V \approx -2$ . This is because the static mean-field is insensitive to changes of the hopping  $t$  in the insulating phases. On the contrary, within the B-DMFT method the dependence on the hopping amplitude in the insulating phases is preserved. Hence, in the top panel of Fig. 1, the line separating DW and MI phases is not exactly flat but varies slightly with changing  $t$ .

The second discrepancy requires a more detailed study of the behavior of the order parameter in the vicinity of the phase transition lines. In the static mean-field study it has been observed that the type of the phase transition depends on the point at which we cross the phase boundary.<sup>8,9</sup> E.g., for  $U/t \approx 14.7$  and  $-U/V \approx -1.67$  the phase transition between SS and DW 2-0 phases is continuous. At the same time, for  $U/t \approx 14$  and  $-U/V \approx -1.56$  the phase transition between SS and

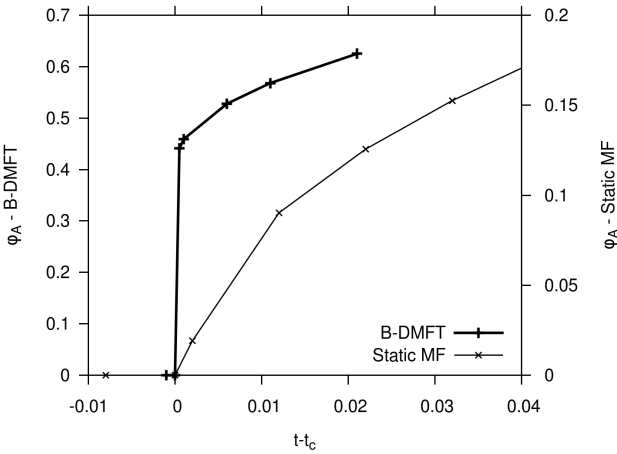


FIG. 2. Dependence of the order parameter  $\phi_A$  (of the doubly occupied site) on the relative hopping amplitude  $t - t_c$  for  $V = 6$  at the phase transition between SS and DW. Thick line with +'s represents results obtained with the B-DMFT method. Thin line with x's represents results obtained with the static mean-field method. Apart from the different magnitude of  $\phi_A$  obtained with the two methods, reflected by different scales on the graph, we observe that the behavior around critical point is significantly different. It seems, that  $\phi$  is discontinuous in the B-DMFT, contrary to the static-mean-field results.

DW 3-0 phases is discontinuous. Within our method this seems not to be the case. Every phase transition, except for the one between SF and MI, is discontinuous. This is particularly interesting for the transition from SS to DW 2-0 phase, because it shows the difference between the static mean-field and the B-DMFT results. The behavior of the order parameter close to the phase transition is depicted in Fig. 2. In the B-DMFT the drop of the order parameter seems to be abrupt at the critical value of the hopping amplitude,  $t_c$ . On the contrary, the behavior in the static mean-field is clearly continuous. However, this statement is based on numerical data and one cannot exclude a very steep yet continuous behavior. In fact, trying to fit a power law dependence  $\phi_A \sim |t - t_c|^a$  to our data gives  $a \sim 0.05$ . Even though such fit includes only first two points above  $t_c$  and that the value of  $t_c$  could be underestimated, there could in principle be a power law dependence with  $a \leq 0.05$ . Performing calculations closer to critical point within our, CT-QMC, method is impractical, because it suffers from the critical slowing down.

It is also interesting to investigate the behavior of the order parameters within the SS phase. Particularly intriguing is the dependence of  $\phi_A - \phi_B$  on the infinite-range interaction strength  $V$  in the region presented in the inset of Fig. 1, top panel. The quantity  $\phi_A - \phi_B$  as a function of  $V$  is plotted in Fig. 3. The behavior is non-monotonic and seems to have a sharp “kink”. A more detailed study, with a finer grid, shows that neither the derivative of  $\phi_A - \phi_B$  nor the other order parameters, e.g.,

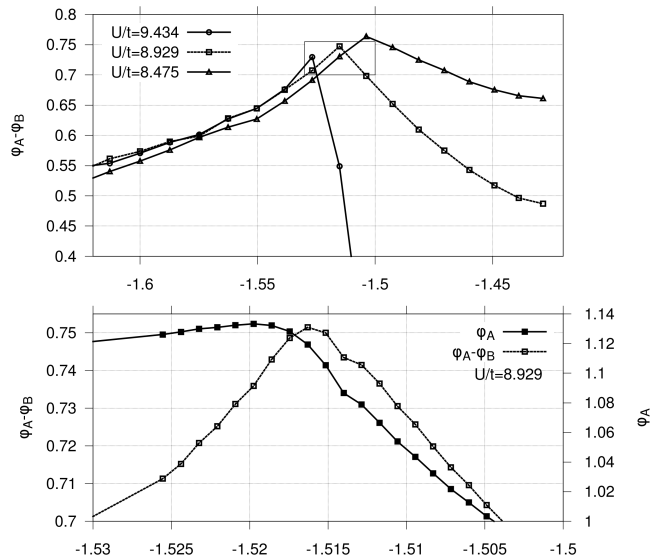


FIG. 3. Top panel: dependence of  $\phi_A - \phi_B$  (difference of order parameters on sublattices A and B) on infinite-range interaction term  $V$  for several values of  $U/t$ , c.f., inset in Fig. 1, top panel. One can observe a sudden change of the slope of the function as  $V$  increases. Bottom panel: A more detailed plot around the kink of  $\phi_A - \phi_B$  for  $U/t = 8.929$  and comparison to behavior of the SF order parameter on sublattice A.

$\phi_{A/B}$ , are discontinuous, c.f., Fig. 3, bottom panel. We also do not detect any change in the symmetry of the solution. Therefore, we conclude that the “kink” does not represent a true phase transition but merely a crossover between a SS with  $\Delta n \approx 2$  and a SS with  $\Delta n \approx 3$ . This represents one more difference between the B-DMFT and the static mean-field results.<sup>9</sup> Namely, in the latter the SS is not a single phase but it splits into two (or more) phases separated by a phase transition line ending in a critical point, c.f., Fig. 1, bottom panel.

## B. Spectral functions

In the following we present the spectral functions of the model (1). We skip the discussion of the problem in the MI and SF phases since it has been already thoroughly studied.<sup>16,21–27</sup> On the other hand, the spectral functions of the SS and DW phases have not been investigated in details yet. The only study we are aware of is the one within the static mean-field approximation and only for the lowest-energy excitations.<sup>9</sup> In order to elaborate on that subject further we consider two types of spectral functions:

- local density of states  $A_{A/B}(\omega) = -\frac{1}{\pi} \text{Im}[G_{ii}(\omega)]$ , where  $G_{ii}(\omega)$  is the local Green function; subscript A or B specifies the sublattice to which  $i$  belongs,

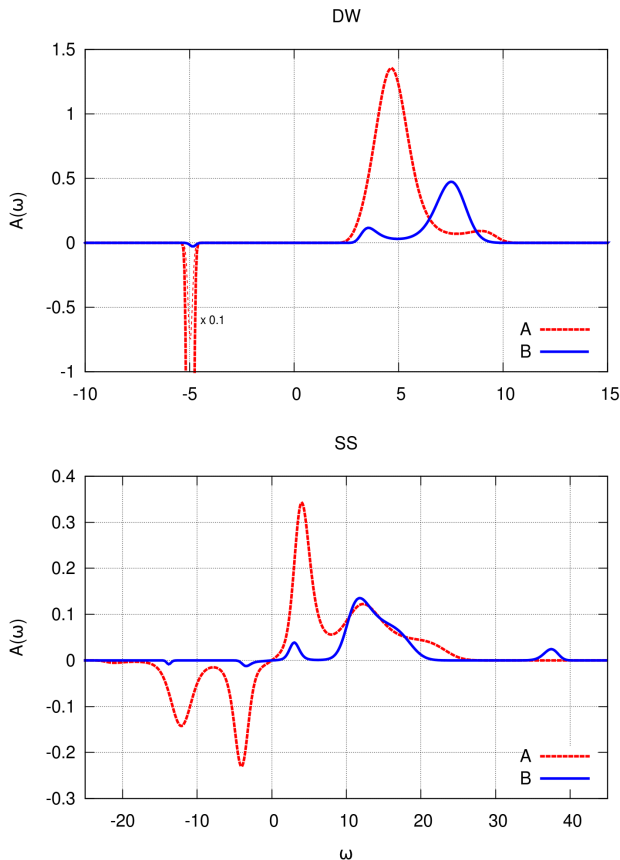


FIG. 4. Local densities of states  $A(\omega)$  of the Bose-Hubbard model with infinite-range interaction. Parameters are set to  $U = 10$ ,  $\beta = 2$  and  $\mu = 4$ . The values of  $t$  and  $V$  are: MI –  $t = 0.4$ ,  $V = 5.5$ ; SS –  $t = 1.12$ ,  $V = 6.555$ . See Fig. 1 for reference. Top panel: Spectral function for the DW. Bottom panel: Spectral function for the SS.

- *momentum resolved spectral function*  $A_\alpha(\mathbf{k}, \omega) = -\frac{1}{\pi} \text{Im}[G_\mathbf{k}^\alpha(\omega)]$ , where the Green function  $G_\mathbf{k}^\alpha(\omega)$  is represented in the basis of operators  $\hat{b}_{\mathbf{k},1}$  and  $\hat{b}_{\mathbf{k},2}$  which diagonalizes the noninteracting Hamiltonian, hence the index  $\alpha \in \{1, 2\}$ . Transformation to this basis from the initial one, used in the Hamiltonian (1), involves separate Fourier transforms for sublattices  $A$  and  $B$  and then some mixing for a given value of quasi-momentum  $\mathbf{k}$ . Notice that since the lattice is bipartite, the area of the Brillouin zone (BZ) is reduced by half.

Within the B-DMFT method we obtain Green functions on the imaginary axis  $G(i\omega_n)$ . In order to determine the Green functions on the real axis  $G(\omega)$  we need to perform analytic continuation. We use the *maximum entropy*<sup>28</sup> method for the numerical analytic continuation since within the CT-QMC we obtain results for finite number of frequency points and with a stochastic noise. More details on the data preparation and obtaining spectral functions within the B-DMFT can be found in Ref. 16.

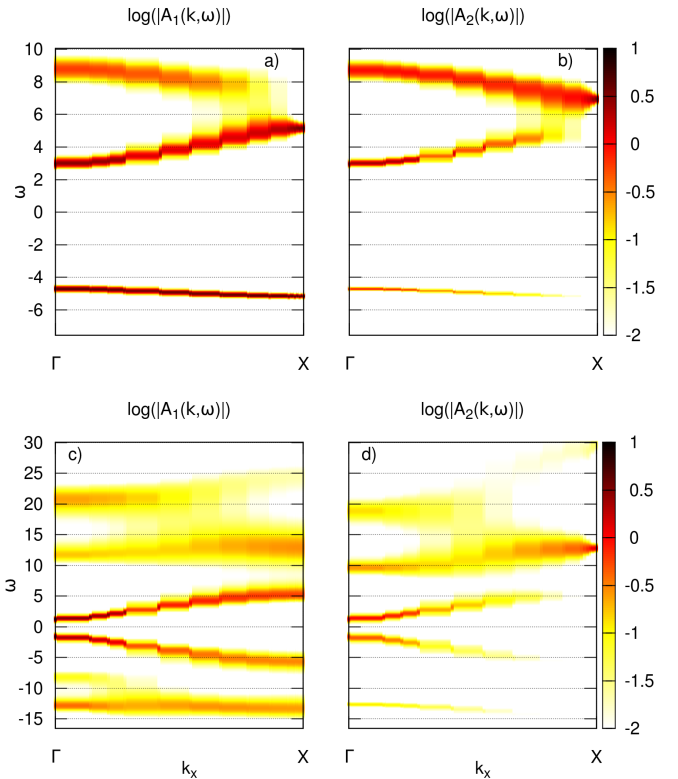


FIG. 5. Momentum resolved spectral functions  $A(\mathbf{k}, \omega)$  of the Bose-Hubbard model with infinite-range interactions for the DW phase (top panels) and the SS phase (bottom panels). Lower index of  $A$  denotes one of two states with quasi-momentum  $k$ , which diagonalize the non-interacting problem. Note the logarithmic color scale.

In Fig. 4 we present results for the local density of states  $A(\omega)$  for both sublattices, where  $A$  is occupied and  $B$  is nearly empty. The parameters were set to  $U = 10$ ,  $\mu = 4$  and  $\beta = 2$ . We set  $t = 0.4$ ,  $V = 5.5$  to obtain the DW phase and  $t = 1.12$ ,  $V = 6.555$  to get the SS phase (see Fig. 1 for reference). The results for the former are presented in the top panel. In this case the average occupation on different sites are  $n_A = 1.9906$  and  $n_B = 0.0096$ , which means that one sublattice is almost doubly occupied at each site and the other is nearly empty. We distinguish three peaks, which we call bands on the basis of the momentum resolved spectral functions analysis, which will be discussed later. Two of those are particle bands and appear for positive values of  $\omega$  and one is a narrow hole band appearing for negative values of  $\omega$ . The distance between the center of hole and the center of particle bands is approximately equal to the interaction strength  $U = 10$ . The hole band centers at around  $\omega = -5$ . It has a form of a narrow peak and is present for both sublattices, however, its weight is significantly smaller for the sublattice  $B$ . This is because creation of a hole can occur only on the occupied site. Hence the peak is suppressed for the nearly empty sublattice  $B$ . The small width of the band comes from the fact that

holes are localized on the sublattice  $A$ , bound to it due to absence of particles on sublattice  $B$ . This means that their dependence on quasi-momentum is weak.

Let us consider the two particle bands. For the occupied sublattice  $A$  more of the spectral weight is distributed to the band with lower energies, concentrating between  $\omega = 3$  and  $\omega = 6$ . We also see a shoulder corresponding to the second band with higher energies. Conversely, on the empty sublattice we observe more of the spectral weight distributed to the higher energy band, spanning between  $\omega = 7$  and  $\omega = 9$  and a shoulder corresponding to the lower energy excitations. The fact that the bands are not completely separated can be attributed to the finite resolution of *maximum entropy* and/or to a finite temperature.

This behavior can be understood on a basis of the local problem with  $t = 0$ . For given parameters and average occupations we have  $V(n_A - n_B) \approx 11$ . This would give two excitations on the occupied sublattice: hole excitation at  $\omega = -5$  with  $A(\omega) = -2\delta(\omega + 5)$  and particle excitation at  $\omega = 5$  with  $A(\omega) = 3\delta(\omega - 5)$ . Similarly, on the empty sublattice this gives a particle excitation at  $\omega = 7$  with  $A(\omega) = \delta(\omega - 7)$ . The nonzero value of  $t$  results in broadening of the bands compared to the local problem, the lower band extends towards lower energies and the higher band, towards higher energies.  $t \neq 0$  also results in some exchange of particles between sublattices hence the states become mixed and we see signatures of excitations corresponding to the  $B$  sublattice on the sublattice  $A$  and vice versa.

Next we consider the results for the SS phase, for which  $n_A \approx 2.45$  and  $n_B \approx 0.2$ . They are presented in Fig. 4 bottom panel. The bands are much wider because the hopping amplitude is larger than in the previous case. This is most prominent for the negative part of the spectrum of the sublattice  $A$ . In the DW phase we observed localized hole excitations, hence a narrow band. In the SS phase the interpretation of the part of spectrum with  $\omega < 0$  as hole excitations loses its virtue. This is due to the presence of the condensate:  $\phi_A^2 \approx 1.27$  and  $\phi_B^2 \approx 0.17$  and, as a result, fluctuating number of particles in the system  $\langle \hat{b} \rangle \neq 0$ . The elementary excitations combine the properties of both particles and holes, e.g., the Bogoliubov quasi-particle operator is a superposition of creation and annihilation operator.<sup>29</sup> Therefore, for each excitation with energy  $\omega$  its spectral weight will be distributed between the peaks at  $\omega$  and  $-\omega$ . The spectrum for the sublattice  $B$  looks significantly different. The negative and low energy part of the spectrum appears only due to the mixing of states on the sublattices  $A$  and  $B$ . The main part of the spectrum starts at around  $\omega = 10$ , which coincides with energy of adding a particle on an empty site of the sublattice  $B$  with  $V(n_A - n_B) \approx 14.4$ ,  $\mu = 4$  and for  $t = 0$ . One can interpret the spectrum  $B$  as particle excitations with high energy  $\omega > 10$ , and some quasi-particle excitations for lower energies, due to their exchange with the sublattice  $A$ .

In Fig. 5 we present the momentum resolved spectral functions  $A(\mathbf{k}, \omega)$ . Due to the bipartiteness of the lattice the Brillouin zone (BZ) is reduced and, as a result, one needs two types of states for each value of the quasi-momentum. The operators for these states are chosen such that the Hamiltonian (2) without local interaction is diagonal in the new basis. We plot our results along special line in the reduced BZ (between special points  $\Gamma = (0, 0)$  and  $X = (\pi/2, \pi/2)$ , assuming that lattice constant is equal to unity). As previously, we first analyze the results in the DW phase, shown in Fig. 5 a) and b). The two plots correspond to two different operators for given quasi-momentum  $\mathbf{k}$ . The results are consistent with those of a local spectral function. We observe a narrow band (the dependence on  $\mathbf{k}$  is weak) for the negative  $\omega$ . For the positive values of  $\omega$  we observe two bands, one stretching from  $\omega \approx 3$  to  $\omega \approx 5$  and one from  $\omega \approx 7$  to  $\omega \approx 9$ . This is consistent with the results for the local spectral function, shown in Fig. 4. One should also notice that the gap between the two particle bands is equal to  $2(V(n_A - n_B) - Un_A) = 2$ . The same result would be obtained if we treated the interaction within the Hartree-Fock approximation. Therefore the DW phase can be well understood on the basis of a simple static mean-field consideration.

The plot of  $A(\mathbf{k}, \omega)$  looks significantly different in the SS phase, shown in Fig. 5 c) and d). Firstly we observe two low energy bands. These bands seem to be symmetric with respect to  $\omega = 0$  axis. The energy of the excitations becomes small as we approach the  $\Gamma$  point, almost reaching  $\omega = 0$ . These low energy excitations originate on the sublattice  $A$ . The states of a local problem with occupation of 2 and 3 particles have similar energy. Therefore, the energetic cost of creating excitation by adding or removing a particle is low. The fact that these bands are symmetric was explained earlier: it is related to the quasi-particle excitations which are superposition of particles and holes. The open gap between the lowest energy bands (around  $\omega = 0$ ) is a feature of the B-DMFT approach. It appears because in the B-DMFT the Hugenholtz-Pines theorem<sup>30</sup> is not satisfied.<sup>13,16</sup> In fact we would expect not only a closed gap, but also linear dispersion relation as we approach  $\omega = 0$ . We also observe three higher energetic bands, two for positive and one for negative  $\omega$ . Two of those can also be related, though not in one to one correspondence, to the excitations of a system in the atomic limit. E.g., the energy of  $\omega \approx 10$  is similar to adding a 4<sup>th</sup> particle on the sublattice  $A$  or a particle on the sublattice  $B$ , and for  $\omega \approx 20$  can be interpreted as adding a 2<sup>nd</sup> particle on the sublattice  $B$  (if the site is already occupied).

It is worth noticing, that in the DW phase low-energy particle band has energy  $\omega$  increasing with quasi-momentum  $\mathbf{k}$ , while the other particle band has energy decreasing with quasi-momentum. It seems not to be the case this in the SS phase. For the two lowest energy bands with  $\omega > 0$  the energy increases with quasi-momentum. This is due to the fact that mixing of states on sublat-

tices is more efficient for states with similar energies. In this case, excitations with similar energy are: (i) adding a 4<sup>th</sup> particle on triply occupied site of the sublattice *A*, (ii) adding a particle on empty site of sublattice *B*. In both cases the energy of creating such excitation is  $\omega \sim 10$ . In such case we would expect the band with inverted dependence on quasi-momentum to appear for even higher energies, which is not determined reliably within our method. This means that high energy features of the graph can also represent a signature of this kind of excitation.

Finally, some features of Fig. 5 are difficult to explain on a simple mean-field level. E.g., the band at  $\omega \approx -13$  is narrow and significantly more visible in  $A_1(\mathbf{k}, \omega)$ , which corresponds more to the sublattice *A*. This would suggest, that it represents creating a hole on the sublattice *A*, which cannot propagate through the system, because sublattice *B* is scarcely occupied. However, the energy  $\omega \approx -13$  does not support such an interpretation.

#### IV. SUMMARY

In summary, we have presented a thorough study of the Bose-Hubbard model with infinite-range interactions mediated by the cavity light modes. The use of the B-DMFT, which is a dynamical method, allows us to obtain a more reliable phase diagram. Because in the problem we need to take into account that the square lattice becomes bipartite, we have derived and used an appropriate full self-consistency relation. The main result is the phase diagram, which qualitatively agrees with the experimental results. Comparison with other mean-field

theoretical results shows both similarities and disagreements between the two approaches. While the phase diagram looks qualitatively similar, some phase transitions are of different type. We have also found an interesting behavior within the supersolid phase, which could be a precursor of a phase transition at zero temperature.

Apart from phase diagram we have studied the spectral properties of the supersolid and density wave phases. We have presented both local and momentum resolved spectral functions. We have analyzed our results finding similarities with simple expansion around the atomic limit in small *t* parameter, hoping to give some intuitive understanding of processes occurring in system with infinite-range interaction mediated by the cavity light mode.

#### ACKNOWLEDGMENTS

The authors would like to acknowledge fruitful discussions with J. Kuneš, J. Skolimowski and D. Vollhardt. Support by the Deutsche Forschungsgemeinschaft through TRR 80 (K. B.) is acknowledged.

#### Appendix A: B-DMFT self-consistency for a bipartite lattice

In order to close the self-consistency of the B-DMFT we need to obtain the full Green function based on the local impurity results. Within the B-DMFT approximation one uses Dyson equation

$$\mathbb{G}_{ij}^{-1}(i\omega_n) = \begin{pmatrix} (i\omega_n + \mu - V_i^{eff} - \Sigma_i^{11}(i\omega_n))\delta_{i,j} - t_{ij} & -\Sigma_i^{12}(i\omega_n)\delta_{i,j} \\ -\Sigma_i^{21}(i\omega_n)\delta_{i,j} & (-i\omega_n + \mu - V_i^{eff} - \Sigma_i^{22}(i\omega_n))\delta_{i,j} - t_{ij} \end{pmatrix}, \quad (A1)$$

where we use similar notation as in Ref. [16], Green function is in Nambu notation,  $\Sigma(i\omega_n)$  are matrix elements of the self-energy  $\Sigma$  (further on, for brevity, we do not write explicitly that  $\Sigma$  depends on frequency),  $V^{eff} = V(n_A - n_B)$  is the effective potential due to infinite-range interaction *V*, and  $\omega_n$  are Matsubara frequencies. This general expression can be significantly simplified in the case of bipartite lattice because then the self-energy and local potential are expressed as

$$\begin{aligned} \Sigma_i &= \bar{\Sigma} \pm \delta\Sigma, \\ V_i^{eff} &= \pm V^{eff}, \end{aligned} \quad (A2)$$

where we have '+' sign for sublattice *A* and '-' sign for sublattice *B*,  $\bar{\Sigma}$  and  $\delta\Sigma$  are halved sum and difference of self-energies on sublattices *A* and *B*. Since the system is homogeneous we perform a Fourier transform. For

convenience we choose the wave-vectors in the same way as for the system, where there is no difference between sublattices (notice, that this convention is different than the one used for spectral functions, see Sec. III B)

$$\mathbb{G}_{\mathbf{k},\mathbf{q}}^{-1} = \sum_{i,j} \begin{pmatrix} e^{i\mathbf{k}\mathbf{R}_i} & 0 \\ 0 & e^{i\mathbf{k}\mathbf{R}_i} \end{pmatrix} \mathbb{G}_{ij}^{-1} \begin{pmatrix} e^{-i\mathbf{q}\mathbf{R}_i} & 0 \\ 0 & e^{-i\mathbf{q}\mathbf{R}_i} \end{pmatrix} / N. \quad (A3)$$

As a result we obtain the following expression

$$\begin{aligned} \mathbb{G}_{\mathbf{k},\mathbf{q}}^{-1}(i\omega_n) &= \\ (i\omega_n \sigma_3 + (\mu - \epsilon_k) \mathbb{1} - \bar{\Sigma}) \delta_{\mathbf{k},\mathbf{q}} &- (\delta\Sigma + V^{eff}) \delta_{\mathbf{k},\mathbf{q}+\pi} \end{aligned} \quad (A4)$$

where  $\epsilon_k = \sum_j t_{ij} e^{ik(R_i - R_j)}$  and  $\pi = (\pi, \pi)$  is a vector corresponding to the special point *M* in Brillouin zone of a 2D lattice (lattice constant is set to unity). We notice,

that the expression, apart from mixing pairs of states  $\mathbf{k}$

and  $\mathbf{k} - \pi$ , separates for different  $k$ 's. Inverting the above formula we obtain

$$\mathbb{G}_{\mathbf{kq}}(i\omega_n) = \left\{ [\mathfrak{G}_3 i\omega_n + (\mu - \epsilon_{\mathbf{k}}) \mathbb{1} - \bar{\Sigma}] - (\delta \Sigma + \mathbb{V}^{eff}) [\mathfrak{G}_3 i\omega_n + (\mu - \epsilon_{\mathbf{k}-\pi}) \mathbb{1} - \bar{\Sigma}]^{-1} (\delta \Sigma + \mathbb{V}^{eff}) \right\}^{-1} \times \\ (\delta_{\mathbf{k},\mathbf{q}} \mathbb{1} + (\delta \Sigma + \mathbb{V}^{eff}) [\mathfrak{G}_3 i\omega_n + (\mu - \epsilon_{\mathbf{k}-\pi}) \mathbb{1} - \bar{\Sigma}]^{-1} \delta_{\mathbf{k}-\pi,\mathbf{q}}). \quad (\text{A5})$$

This expression can now be easily Fourier-transformed back, according to Eq. A3, to the real-space, yielding lattice Green function, in particular its local part  $\mathbb{G}_{ii}(i\omega_n)$ .

- <sup>1</sup> M. Greiner, O. Mandel, T. Esslinger, T. W. Hänsch, and I. Bloch, *Nature* **415**, 39 (2002).
- <sup>2</sup> I. Bloch, J. Dalibard, and W. Zwerger, *Rev. Mod. Phys.* **80**, 885 (2008).
- <sup>3</sup> D. Jaksch, C. Bruder, J. I. Cirac, C. W. Gardiner, and P. Zoller, *Phys. Rev. Lett.* **81**, 3108 (1998).
- <sup>4</sup> H. Ritsch, P. Domokos, F. Brennecke, and T. Esslinger, *Rev. Mod. Phys.* **85**, 553 (2013).
- <sup>5</sup> R. Landig, L. Hrúby, N. Dogra, M. Landini, R. Mottl, T. Donner, and T. Esslinger, *Nature* **532**, 476 (2016).
- <sup>6</sup> M. P. A. Fisher, P. B. Weichman, G. Grinstein, and D. S. Fisher, *Phys. Rev. B* **40**, 546 (1989).
- <sup>7</sup> Y. Li, L. He, and W. Hofstetter, *Phys. Rev. A* **87**, 051604(R) (2013).
- <sup>8</sup> Y. Chen, Z. Yu, and H. Zhai, *Phys. Rev. A* **93**, 041601 (2016).
- <sup>9</sup> N. Dogra, F. Brennecke, S. D. Huber, and T. Donner, arXiv, 1604.00865v1.
- <sup>10</sup> K. Byczuk and D. Vollhardt, *Phys. Rev. B* **77**, 235106 (2008).
- <sup>11</sup> A. Kauch, K. Byczuk, and D. Vollhardt, *Phys. Rev. B* **85**, 205115 (2012).
- <sup>12</sup> M. Snoek and W. Hofstetter, “Quantum gases: Finite temperature and non-equilibrium dynamics,” (Imperial College Press, London, 2013) Chap. 1, pp. 355–365.
- <sup>13</sup> P. Anders, E. Gull, L. Pollet, M. Troyer, and P. Werner, *New J. Phys.* **13**, 075013 (2011).
- <sup>14</sup> P. Anders, E. Gull, L. Pollet, M. Troyer, and P. Werner, *Phys. Rev. Lett.* **105**, 096402 (2010).
- <sup>15</sup> A. Georges, G. Kotliar, W. Krauth, and M. J. Rozenberg, *Rev. Mod. Phys.* **68**, 13 (1996).
- <sup>16</sup> J. Panas, A. Kauch, J. Kuneš, D. Vollhardt, and K. Byczuk, *Phys. Rev. B* **92**, 045102 (2015).
- <sup>17</sup> J. W. Negele and H. Orland, *Quantum Many-Particle Systems* (Addison-Wesley, Melno Park, 1988).
- <sup>18</sup> E. Gull, A. J. Millis, A. I. Lichtenstein, A. N. Rubtsov, M. Troyer, and P. Werner, *Rev. Mod. Phys.* **83**, 349 (2011).
- <sup>19</sup> N. V. Prokof'ev, B. V. Svistunov, and I. S. Tupitsyn, *JETP* **87**, 310 (1998).
- <sup>20</sup> Notice, that for  $t = 0$  static mean-field and the B-DMFT are equivalent.
- <sup>21</sup> S. D. Huber, E. Altman, H. P. Blücher, and G. Blatter, *Phys. Rev. B* **75**, 085106 (2007).
- <sup>22</sup> K. Sengupta and N. Dupuis, *Phys. Rev. A* **71**, 033629 (2005).
- <sup>23</sup> N. Dupuis, *Phys. Rev. Lett.* **102**, 190401 (2009).
- <sup>24</sup> A. Sinner, N. Hasselmann, and P. Kopietz, *Phys. Rev. Lett.* **102**, 120601 (2009).
- <sup>25</sup> M. Knap, E. Arrigoni, and W. von der Linden, *Phys. Rev. B* **83**, 134507 (2011).
- <sup>26</sup> T. A. Zaleski, *Phys. Rev. A* **85**, 043611 (2012).
- <sup>27</sup> H. U. R. Strand, M. Eckstein, and P. Werner, *Phys. Rev. A* **92**, 063602 (2015).
- <sup>28</sup> M. Jarrell and J. E. Gubernatis, *Phys. Rep.* **269**, 133 (1996).
- <sup>29</sup> H. Shi and A. Griffin, *Phys. Rep.* **304**, 1 (1998).
- <sup>30</sup> N. M. Hugenholtz and D. Pines, *Phys. Rev.* **116**, 489 (1959).